Health monitoring of aerospace structures utilizing novel health indicators extracted from strain and acoustic emission data

Georgios Galanopoulos[1], Agnes Broer[2], Dimitrios Milanoski[1], Dimitrios Zarouchas[2], Theodoros Loutas[1*]

[1] Applied Mechanics Laboratory, Department of Mechanical Engineering and Aeronautics, University of Patras, Rio, Greece

[2] Structural Integrity and Composites Group, Faculty of Aerospace Engineering, Delft University of Technology, Delft, The Netherlands

* Corresponding Author - Email address: thloutas@upatras.gr (T. Loutas)

Abstract:

Health Indicators (HI) of diagnostic potential extracted from raw sensor data is an essential feature for data-driven diagnostics and prognostics of composite structures. In this paper, new damage sensitive features, developed from strains acquired with Fiber Bragg Grating (FBG) and Acoustic Emission (AE) data, are investigated for their suitability as HIs. Two fatigue test campaigns are conducted on single-stringered composite panels. After an initial damage introduction in the form of either impact damage or artificial disbond, the panels are subjected to constant and variable amplitude compression-compression fatigue tests. Strain sensing through FBGs and AE, two promising Structural Health Monitoring (SHM) techniques, are employed to monitor the damage growth which is further verified by phased array ultrasound. Several FBGs are incorporated in special SMARTapes™ which are bonded along the stiffener's feet to measure the strain field, while the AE sensors are strategically placed on the panels' skin to record the acoustic emission activity. Several HIs are extracted from FBGs and AE raw data with promising behavior for damage monitoring of composite structures during service. To further assess the HIs behavior and suitability, measurements with a phased array camera at several time instances throughout the course of the experiments provide with ultrasound-based estimations of damage.

Keywords: Structural Health monitoring, Composite stiffened panels, FBG sensing, Acoustic emission, Health Indicators

1. Introduction

Composite materials are being increasingly used as structural components in many applications. In the aeronautics industry, modern aircraft structures consist of more than 50% of composite materials [1], due to their unique property of high strength to weight ratio, as well as enhanced corrosion resistance. However, the non-homogeneous nature of these materials involves complex and not yet perfectly understood degradation and failure processes. These structural components are constantly subjected to variable service loads and environmental loadings which can greatly reduce their load bearing capability and at occasions cause damage that fails to be identified during routine inspections. A good example of such damage is Barely Visible Impact Damage (BVID), which causes subsurface damage which is critical to the structure's integrity[2]. Structural Health

Monitoring (SHM) technology has been introduced and evolved the last 30 years with the aim to detect, locate and quantify the degradation of a structure [3]. The last few years a trend emerges towards an even more demanding task, the utilization of SHM data towards the intelligent prognosis of the structure's remaining useful life [4, 5]. SHM as utilized via a network of sensors attached strategically to a structure can ultimately lead to the implementation of a Condition-Based Maintenance (CBM) paradigm, significantly reducing downtime-induced delays and unscheduled maintenance costs as well as increasing safety[6]. Regarding the SHM technologies currently being mostly sought by the research community, we may refer to Fiber Optic Sensors (FOS) for strain sensing, piezo-electric elements for Lamb wave testing, comparative vacuum monitoring, acoustic emission (AE), vibration testing etc.

FOS are a state-of-the-art sensing technology able to monitor composite structures. Their tolerance to electromagnetic interferences as well as environmental conditions offer great flexibility for use in various applications. FOS, Fiber Bragg Gratings (FBG) especially, have attracted the interest of many researchers and have been applied to various fields. Milanoski and Loutas [7], studied numerically a composite single stringered panel with the use of virtual FBGs. They developed strain-based health indicators (HIs) for skin-stiffener disbond monitoring. Palaniappan et al. [8], used embedded chirped FBGs to monitor disbonds on adhesively bonded composite joints. It was observed that initiation of disbond growth would cause a wavelength shift at the sensor located closer to that disbond. On another research, Li et al. [9], created an automated algorithm to detect disbonds using FBG strain measurements on GFRP T-joints on naval structures. Both the virtual finite element and the experimental strain showed alteration of the strain field near disbond locations. Kahandawa et al. [10], studied extensively the effects of various loading conditions on the strain readings of FBGs. They used an Artificial Neural Network (ANN) to predict damage evolution in the structure using FBG readings as the indicator of damage. Sundaram et al. [11] used strain data from both experimental readings and Finite Element Models (FEM) to train a NN to monitor and determine damage size. The authors used both strain gauges and FBGs to monitor the strains and observed that both methods provided similar strain readings. Takeda et al. [12] used embedded FBGs to monitor the central wavelength reflection spectra during impact damage on composite panels. It was shown that the wavelength spectra was permanently altered after the impact. Airoldi et al. [13] used FBG readings to monitor load and damage progression on composite wing-box's spars. Sbaruffati et al. [14] proposed a damage detection method using Mahalanobis distance. The method was first implemented on a finite element model of a helicopter tail to monitor fatigue crack propagation. To validate the method an experiment with permanently bonded FBG sensors to record strains was conducted. Also, Sbaruffati et al. [15] proposed a methodology for crack damage diagnostics based on a normalized strain damage index. ANNs were used for the diagnostics trained based on experimental and FEM data. Tur et al. [16] used FBG and DFOS to detect and monitor impact damage on composite stiffened panels during a static compression loading. It was observed that the strains on the impacted stringer largely deviated from those of an un-impacted one, especially with increasing load. On another research, Guemes et al. [17], used FBG sensor readings with PCA to detect different types damage on a composite wing spar. T^2 index and Q index were used to discern the different damage cases. Also, Guemes et al.[18] used FOS (both distributed and FBG) to monitor damage in composite structures. Damage was identified but the location and size of the damage in conjunction with the sensor location played an important part.

AE is also a powerful SHM solution, which has been extensively used in literature [19]. Zhou et al. [20] used acoustic emission with DIC to monitor the compressive behavior of multi delaminated composites. More specifically, they correlated the amplitude, duration and relative energy with

damage propagation. Also, Masmoudi et al. [21] used AE to identify and compare damage mechanisms and their evolution in 3-point bending fatigue experiments. AE was used to successfully identify the different damage methods and showed that matrix cracking was the dominant failure mechanism, while fiber breaking was the precursor of catastrophic failure. A novel experimental campaign was conducted by Camri et al. [22] on Aluminum-GFRP hybrid specimens with mounted AE sensors. They conducted experiments on both lab scale as well as in scanning electron microscope trying to correlate AE data with the tracking of damage evolution. The use of AE in SHM-based prognostics of the remaining useful life has also been recently studied. Loutas et al. [4] and Eleftheroglou and Loutas [5], used acoustic emission features as damage indicators for remaining useful life prediction on composite open-hole specimens. It was observed that the windowed cumulative rise time to amplitude ratio (RA) has a monotonic trend and can be used for prediction tasks. The same was observed for the windowed cumulative energy. Liu et al. [23] used acoustic emission data to predict the remaining useful life of composite coupons under cyclic loading. It was concluded that AE could monitor the degradation process, and setting a proper amplitude threshold, greatly improved the process efficiency. Broer et al. [24] has recently proposed a methodology of fusing two SHM techniques, namely AE and strain sensing. The idea of fusing results from several sensors was proposed in order to take advantage of the strengths of both SHM techniques towards more effective damage diagnostics of deteriorating composite panels.

In order, however, to exploit the direct output of a SHM system (i.e. raw sensor data), intelligent data processing and features that capture the degradation process effectively are needed. These features are usually referred to as Health Indicators (HIs). The quality of the HIs' evolution over operational time largely determines the effectiveness of diagnostic systems [24] and affects the performance of the prognostics methodologies [25]. HIs are essentially features that capture the degradation trend of the structure under study. As we have discussed previously in [26], HIs to be potentially used for diagnostic and prognostic tasks should possess the properties of monotonicity, prognosability and trendability. Monotonicity characterizes a general increasing or decreasing trend of the HI, prognosability measures the spread of the HI failure values and trendability indicates whether degradation histories of a specific structure/subcomponent have the same underlying trend. HIs can be divided into two categories as in [27, 28], namely HIs which are directly derived from physical measurements (pHIs), like static or dynamic strains, ultrasound, temperature or a combination of those properties, and virtual health indicators (vHIs) that are not tied to any physical properties like the reconstruction error (Q index) from principal component analysis. An example of a pHI can be found in [29] where axial strain from DIC measurements was used to predict RUL of open-hole composite coupons. Strain HIs have also been developed in [30] to monitor disbond growth in composite stringered panels. These HIs proved capable of capturing the damage growth. VHIs are usually optimized to obtain desirable attributes like monotonicity, trendability and prognosability, which greatly benefit the performance in prognostics as postulated in [26]. Principal Component Analysis (PCA) is frequently used as a way to create vHIs. Loukopoulos et al. [31] applied PCA, specifically T^2 and Q-index, as HIs to predict the RUL of reciprocating compressors. Zhang et al. [32] used wavelet packet decomposition to extract features in combination with PCA to reduce the dimensionality of the data without losing information. The output of the PCA was used as an input to a Back-Propagation ANN to predict machinery failure. In [33] an autoencoder based Recurrent NN (RNN) is proposed for dimensionality reduction into a 2D feature space. An HI is proposed based on a distance metric and a radial basis function normalization scheme for RUL prediction of aircraft engines.

In the present work, we investigate different methods for constructing novel HIs using FBG strain data and AE SHM data acquired from Single Stringered Panels (SSPs) under constant and variable amplitude fatigue testing. The objective is to identify robust and reliable HIs to use in prognostic tasks. As robust and reliable we determine an HI that is monotonic with damage accumulation, consistent, with an easily set failure threshold and that is least affected by variable operating conditions, as well as providing resistance to outliers. The proposed methodology is schematically shown is Figure 1. From fatigue experiments on a generic aircraft element, the raw sensor data are extracted from FBG and AE sensors, and then processed with different approaches. The data are then further processed to create robust HIs with monotonic behaviors linked to the component's degradation. A damage estimation provided by the phased array C-scan is utilized to evaluate the HI's correlation to the evolving damage. The HIs should also poses desirable attributes in order to be employed in prognostics. The remainder of this paper is organized as follows; section 2 provides information on the experimental campaign and data pre-processing; in section 3 the proposed Health Indicators are presented and in section 4 the experimental results are discussed. Finally, the main concluding remarks are given in section 5.

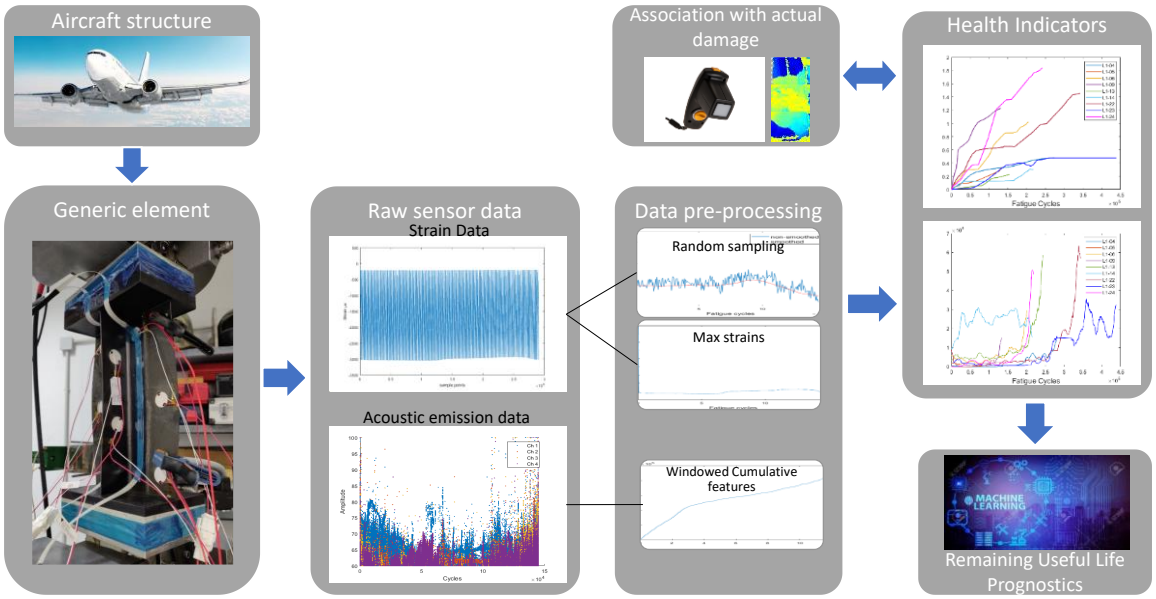

Figure 1: Schematic representation of the proposed methodology

2. Experimental procedure

2.1 Test article definition

Single Stringered Composite panels were manufactured by Optimal Solutions (Portugal). Both the skin and the T-shaped stiffener were manufactured from IM7/8552 carbon reinforced epoxy unidirectional prepreg with $[45/-45/0/45/90/-45/0]_s$ and $[45/-45/0/45/-45]_s$ layups respectively. A schematic of the panel geometry is shown in Figure 2a. Additionally, two resin tabs were placed on the specimens to ensure proper load introduction and uniform loading during the experiments. All tested specimens had some form of initial damage. In few specimens an artificial disbond was

introduced during manufacturing using a Teflon insert of various sizes between the skin and the stiffener, while the rest were impacted at a drop tower with various energies as analyzed in Tables 1 and 2 and with a target to induce BVID.

2.2 Test campaign

Static compression tests with a constant displacement rate of 0.5 mm/min were first conducted to determine the ultimate collapse load of the panels. The average collapse load was 100 kN and this value guided the selection of the fatigue load levels. Two test campaigns were executed in compression-compression (C-C) fatigue, with an R-ratio of 10 and a frequency of 2 Hz. The first campaign was conducted in the Aerospace Structures and Materials Laboratory of Technical University of Delft. The specimens were tested in constant amplitude fatigue on a MTS hydraulic test machine of 500 kN capacity. The second test campaign was conducted in the applied mechanics laboratory of University of Patras and the specimens were tested on variable amplitude fatigue on an INSTRON 8802 with a 250 kN load cell. The load was increasing after arbitrarily selected blocks of constant loading and after checking the damage state as captured by the Phased Array C-scans. The details of each test campaign can be observed in Tables 1 and 2.

Two SHM technologies were employed throughout the tests to monitor the SSPs structural integrity i.e. AE and strain sensing with FBGs. AE was recording continuously during the experiments. In the first campaign, four Vallen VS900-M broadband sensors were used, while in the second campaign two Micro200HF 500-4500 kHz wideband sensors, from Physical Acoustics Corporation were used. The AE sensors were strategically placed on the SSP's skin (Figure 1). An amplitude threshold of 60 dB and 62 dB respectively was set, due to small differences in the machine noise throughout the tests. The strain measurements are not continuous but every 500 cycles, the fatigue test was paused, the specimens were unloaded and then quasi-statically loaded to the absolute maximum fatigue load. During the quasi-static the strain measurements from the FBGs were performed using a two-channel sm130 dynamic interrogator from Micron Optics. The strain data acquisition rate was set at 100 Hz and 5 Hz for the 1st and 2nd test campaign respectively (it was observed after the first campaign that the 100 Hz acquisition was excessive), and the quasi-static load rate was 0.5 mm/min, same as the static tests. The optical fiber (OF) containing the FBGs was embedded in a SMARTape™ [34] for ease of handling purposes, manufactured and provided by SMARTEC(Switzerland). One SMARTape™ was adhered on each foot of the stiffener using a co-polyamide-based adhesive. Each OF entails five equidistant FBG sensors for a total of ten FBGs per coupon. The measurement length was approximately 140 mm focused in the middle section of the specimen, and the FBG spacing is 20 mm. The conversion from wavelength to strain was made using Eq.1:

$$\varepsilon = \frac{\Delta\lambda}{\lambda_0} * f_g \qquad (1)$$

With $f_g = 1.2$ the grating factor provided by the manufacturer. PZT transducers were also placed on the SSPs but are not studied in the current research.

As previously stated, in the variable amplitude fatigue experiments the damage was also monitored via a portable phased array camera. An initial C-scan of the damage area was performed pre-test and every 10,000-20,000 cycles the test paused and the SSP was inspected for damage growth. The outcome of this inspection i.e. how much the damage was growing, informed the decision to

increase the fatigue load level. The phased array images provide quantitative information on the extent of damage.

Table 1: Constant amplitude fatigue test campaign details

Specimen #	**Impact location / disbond**	**Impact energy/ disbond size**	**Load**		**# of cycles to failure**
			Min.	**Max.**	
L1-04	Skin	10 J	-6.5 kN	-65 kN	280,098
L1-05	Stiffener foot	10 J	-6.5 kN	-65 kN	144,969
L1-09	Stiffener foot	10 J	-6.5 kN	-65 kN	133,281
L1-23	Stiffener foot	30 mm	-5.0 kN -6.0 kN[1]	-50 kN -60 kN[1]	438,000

[1] load increased after 100k cycles

Table 2: Variable amplitude fatigue test campaign details

Specimen #	**Impact location / disbond**	**Impact energy/ disbond size**	**Load**		**# of cycles**
			Min.	**Max.**	
L1-06	Stiffener foot	7.4 J	-4.0 kN	-40 kN	10,000
			-4.5 kN	-45 kN	80,000
			-5.0 kN	-50 kN	30,000
			-5.5 kN	-55 kN	70,000
			-6.0 kN	-60 kN	12,300
					202,300
L1-13	Stiffener foot	10 J	-4.0 kN	-40 kN	10,000
			-4.5 kN	-45 kN	80,000
			-5.0 kN	-50 kN	90,000
			-5.5 kN	-55 kN	63,000
					243,000
L1-14	Stiffener foot	10 J	-4.0 kN	-40 kN	10,000
			-4.5 kN	-45 kN	177,000
			-5.0 kN	-50 kN	30,000
					217,000
L1-22	Stiffener foot	30 mm	-3.5 kN	-35 kN	10,000
			-3.9 kN	-39 kN	10,000
			-4.5 kN	-45 kN	10,000
			-5.0 kN	-50 kN	170,000
			-5.5 kN	-55 kN	85,000
			-6.0 kN	-60 kN	60,000
					345,000
L1-24	Stiffener foot	7.37 J	-4.0 kN	-40 kN	20,000
			-4.5 kN	-45 kN	75,000
			-5.0 kN	-50 kN	25,000
			-5.5 kN	-55 kN	62,000
			-6.0 kN	-60 kN	60,000
					242,000

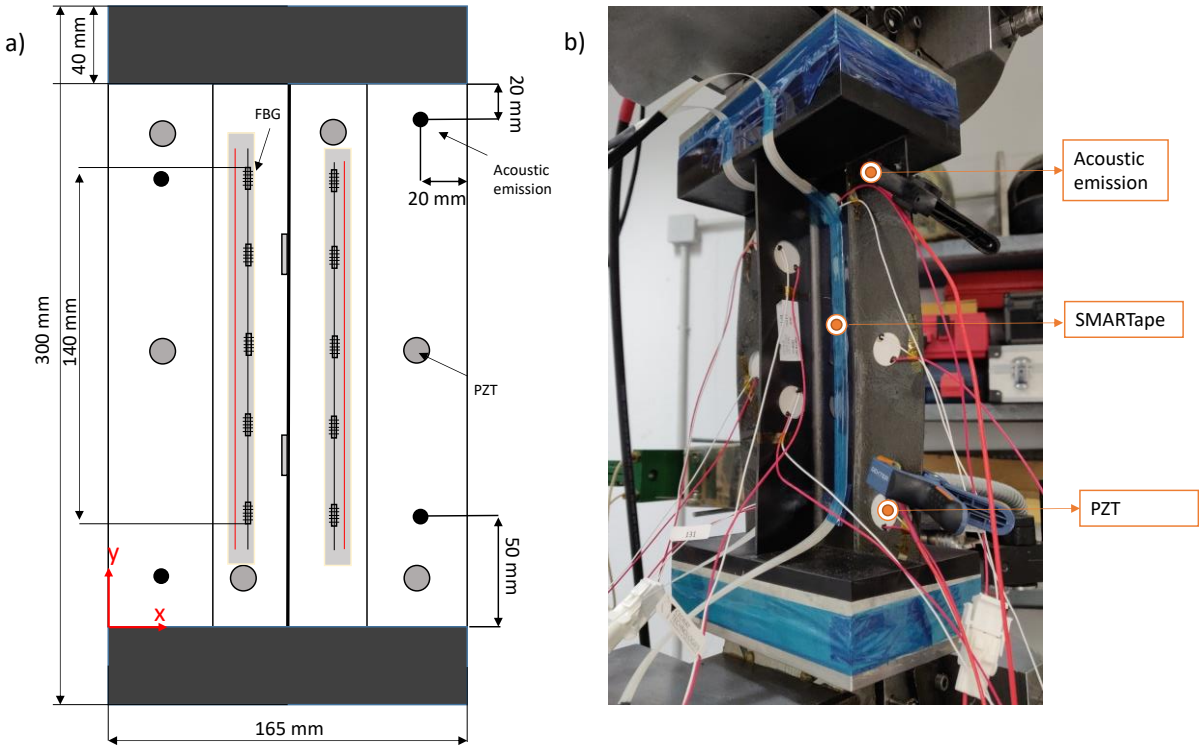

Figure 2: a) Schematic depiction of the SSP and the sensor positioning b) actual test setup

2.3 SHM data pre-processing

The raw SHM data and especially the strain data are quite complex to visualize and uninformative at first glance (Figure 3). Two methods were employed to pre-process the raw strain data before proceeding with the extraction of HIs. The first method utilized the peak strain values at each quasi-static experiment. This is a sensible approach in constant amplitude testing as strain depends apparently on the load. But, in the variable amplitude closer to real-life scenario, the peak strains change not only as the SSP gets damaged, reflecting damage accumulation, but also by the operational load, a change which is not desired. Due to the load level changes in the variable amplitude campaign, steps in peak strain at load changes are observed which in turn negatively affect the HIs evolution. The second method that addresses this issue, involves sampling *n* random samples during the QS loading and calculating the average of these samples as in (2).

$$\varepsilon = avg(\varepsilon_1, \varepsilon_2, \dots, \varepsilon_n) \quad (2)$$

Uniform distribution sampling from the entire quasi-static loading strain measurements was used. The final outcome passed through a moving average filter for smoothening purposes. Smoothening was also applied on the variable amplitude max strain data to lessen the effect of the stepped behavior introduced by the load shifts and make the data more comparable to the constant amplitude fatigue. A graphical representation of the two data processing methods can be seen in Figure 3.

Regarding the AE data pre-processing, due to the multi-gigabyte data from tens of millions of AE hits, a cleaning of the data was first performed, i.e. discarding data recorded during the pauses, e.g. from the load increases during the variable amplitude fatigue experiments or other unexpected pauses. In the second stage, beyond the classical features such as AE hits, counts, duration etc., the

Rise Time/ Amplitude (RA) feature was calculated since it has shown interesting behavior in fatigue tests in previous work [5].

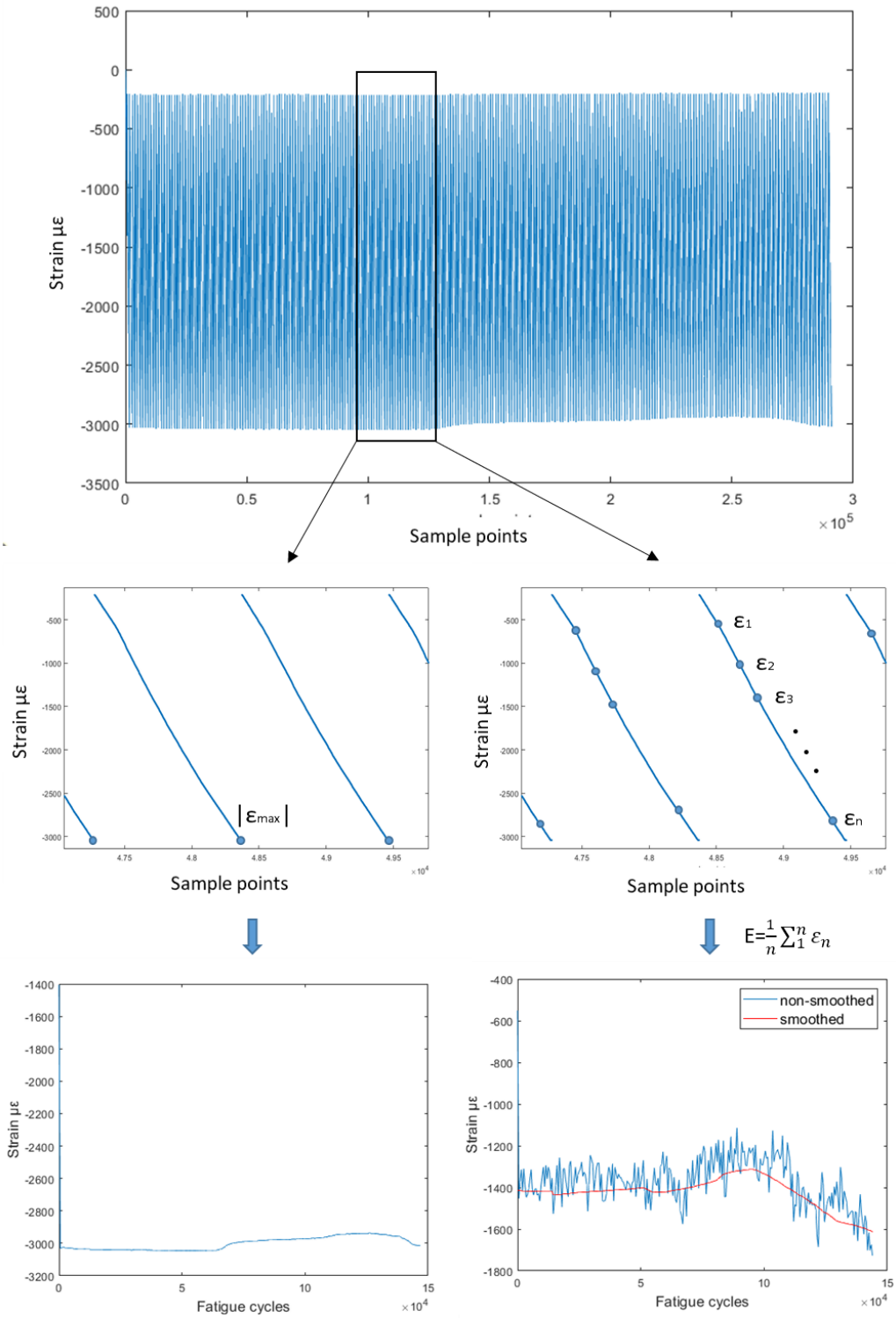

Figure 3: The max strain value from each quasistatic is extracted and creates the strain histories for method 1 (left). n strain points from each quasistatic are randomly sampled and then averaged to create the strain histories for method 2 (right).

3 Methodologies - Health indicator construction

In this section, the proposed HIs will be introduced and described. Two types of HIs are developed, physical HIs, i.e. HIs obtained after simple operations on strain or AE data and virtual HIs, i.e. HIs constructed using more sophisticated processing such as Principal Component Analysis (PCA). PCA is generally used to reduce the dimensionality of the data, by projecting the original data into the principal component space. Each principal component is constructed by a linear fusion of the original variables using the eigenvectors and eigenvalues of the covariance matrix of the original data. PCA and its statistical quantities Q and T^2 have been used in literature for damage diagnostics and prognostics [17, 35, 36].

3.1 Strain based HIs

3.1.1 HI_1

The first proposed HI has been previously used in [7, 37]. In these works, HI_1 was tested on data from both QS simulations conducted in a FEM as well as experiments. It was observed that the HI could capture the existence of damage at increasing loads. HI_1 is given by Eq. (3):

$$HI_1^i(t) = \frac{\left|\varepsilon_{ref}^i - \varepsilon^i(t)\right|}{|\varepsilon_{ref}^i|} \qquad (3)$$

where *i=1, …, N* denotes the i^{th} FBG sensor number among *N* total sensors, *t* is the operational time and ε_{ref}^i is the strain value of sensor *i* at a reference state. Frequently, as reference we assume the strain of a pristine specimen at the same load. However, closer to a real-life scenario where the pristine condition or load may be unknown, we consider as reference the state at the first SHM measurement and this is the rationale behind the proposed assumption. In our case, the reference state is at the starting point for all experiments where damage has been induced (impact or artificial disbond). FBG sensors closer and thus more affected by damage are expected to display higher values. Also, HI_1 for each sensor is only affected by measurements of the studied sensor and eliminates unwanted effects, such as missing data or abnormal behaviors, from the other sensors.

3.1.2 HI_2

The second proposed HI was also introduced and assessed in numerical experiments in [7]. HI_2 combines the strain measurements at all FBGs of the same foot and measures the impact each FBG has on the cumulative strain of the same foot. HI_2 is defined by Eq. (4):

$$HI_2^i(t) = \frac{1}{n}\frac{\varepsilon^i(t)}{\sum_1^n \varepsilon^i(t)} - HI_2^i(0) \qquad (4)$$

Where *i=1, ..., n* denotes the number of sensors on the same foot and *t* is the operational time. The rationale behind HI_2, is that sensors unaffected by damage tend to show minor deviations from the reference condition. The reference value at *t=0* is also subtracted from the subsequent values to allow for an equal assessment. As we shall see later, the strain values at all instances appeared to deviate from the reference, but sensors in the vicinity of damage display higher deviations. HI_2 attempts to highlight this effect.

3.1.3 HI_3

HI_3 is an advancement of HI_2. More specifically, HI_3 is a combination of HI_2 of both right and left feet (RF and LF), i.e. the half-sum of HI_2 at the same height at both feet. HI_3 is defined in Eq. (5):

$$HI_3(t) = \frac{1}{2}[\left(HI_2^i\right)^{RF} + \left(HI_2^i\right)^{LF}] \qquad (5)$$

Where *i=1, ..., n the number of sensors* and *t* is the operational time. HI_3 focuses the damage detection on the horizontal plane created by the two sensors, instead of the exact location a sensor is mounted. This is a useful addition in case the sensor with the damage, on its own, does not provide adequate information. Hence the difference between damaged and undamaged foot may fill the information gap.

3.1.4 HI_4

HI_4 is a fused version of HI_1 for all 10 FBG sensors, aimed at creating a single monotonic indicator. HI_4 is a root squared sum of HI_1 multiplied by a proper weight. As weights, the monotonicity [38] of each HI_1 curve is used, since a major desirable attribute of every HI is a monotonic trend. The HI is squared to ensure that the output is a non-negative number. The general equation of HI_4 is:

$$HI_4(t) = \sqrt{\sum(m_i HI_1^i(t))^2} \qquad (6)$$

where i=1, …, N the number of sensors, m_i the monotonicity of each HI_1^i curve, and *t* is the operational time.

3.2 Virtual Health indicators

As mentioned in the introduction of this section, the virtual HIs in the present work are created using the dimensionality reduction attribute of PCA. Other soft computing approaches such as neural networks or unsupervised clustering can be used as well. PCA is utilized to reduce the available sensor data from 10 variables to up to 3 depending on the explained variance retained in these components.

3.2.1 vHI_1

The first endeavor with the virtual HIs is a modification of the indicator proposed in [33]. In the presented method, the dimensionality of the available sensor data is reduced from 10 to 2 using PCA. The Euclidian distance $d_L(t) = ||Z(t) - Z_0||$ is calculated, where *Z(t)* is the vector of principal components [PC_1(t), PC_2(t)] for the entire lifetime and $Z_0 = Z(t=0)$. A radial basis function is used to normalize the final HI, to ensure that it starts at 1 and fails at $vHI_{1_f} \epsilon [\varepsilon, \varepsilon + \delta]$ with ε=δ=0.01. The rationale of vHI_1 is creating a HI which will be indicative of the degradation process and with appropriate normalization reach a failure point at zero. vHI_1 is given in Eq. (7):

$$\mathrm{vHI}_1(t) = \exp\left(-\frac{(d_L(t) - d_{Lmin})^2}{\sigma_L}\right) \qquad (7)$$

Where,

$$\sigma_L = -\frac{(d_{Lmax} - d_{Lmin})^2}{2}\left[\frac{1}{\log_{10}\varepsilon} + \frac{1}{\log_{10}(\varepsilon+\delta)}\right] \qquad (8)$$

The main drawback of vHI_1 in this current form is the dependence on the knowledge of $d_{Lmin} and\ d_{Lmax}$, a priori. In real cases, these values are unknown but could be estimated from a training dataset.

3.2.2 vHI_2

The second vHI proposed in this section is the so-called Q index or the sum of reconstructed squared residuals of PCA. This was also presented as a feature of diagnostic/prognostic potential alongside Hotelling's T^2 in [31]. The methodology for calculating vHI_2 is as follows:

- The initial portion of the sensor data matrix **X** considered as reference $\mathbf{X}_{ref}$, is normalized to zero mean and unit variance. The mean M_{ref} and the variance V_{ref} are saved for later use.
- A PCA model is created using $\mathbf{X}_{ref}$ and the coefficients matrix $\mathbf{P}_{mxn}$ is calculated, where m is the time points and n the number of sensors. The reduced matrix $\mathbf{P}_{rmxk}$ is saved where k is the number of components who's explained variance is over 90%.
- Then M_{ref} and V_{ref} are used to scale the full dataset **X** and $\mathbf{P}_r$ is used to transform the normalized data $\bar{\mathbf{X}}$ to the PC space as in $\mathbf{T}=\bar{\mathbf{X}}\mathbf{P}_r$.
- Then the reconstructed matrix $\mathbf{X}_r$ is calculated where $\mathbf{X}_r=\mathbf{P}_r^T\mathbf{T}+\mathbf{R}$ and **R** is the reconstruction error.
- Q is calculated in Eq. (9):

$$Q(t) = \sum_1^N \left(x_i(t) - x_{r_i}(t)\right)^2 \qquad (9)$$

Where $i=1, \ldots, N$ the i^{th} FBG sensor and $x_i(t)$ and $x_{r_i}(t)$ the original and reconstructed data at time *t.*

Hotelling's T^2 was also checked but it did not provide any useful information and is not further investigated. Q index, as will be evidenced in section 4, displayed a monotonically increasing behavior over test time, starting from values close to zero.

3.3 Acoustic emission based HIs

A simpler approach was adopted for the HI extraction from the huge amount of raw AE data after each fatigue test. Typically, the AE hits resulted from fatigue tests of SSPs were in the order of 1-15 million. As suggested in [29], windowed cumulative features were extracted from hits and RA. As windowed cumulative features Loutas and Eleftheroglou in [5] defined the sum value of the feature at a specified time window. This way, the randomly recorded AE features obtain a periodic character of values acquired at every time window which is more appropriate for SHM purposes. A variety of different window lengths was tested, and after several trials it was concluded that 500 cycles is a good selection for window size for the aforementioned test campaigns for two reasons. First, it provides a satisfactory increasing trend which is desired for both diagnostic and prognostic purposes. Second, when using 500 cycles as a window, it is possible to directly compare and possibly fuse the AE data with the strain data from FBGs, since they now share the same measurement interval. HI_{AE} at any operational time t is thus calculated as Eq. (10) dictates:

$$HI_{AE}(t) = \sum_{i=t-T}^{t} F(i) \qquad (10)$$

Eq. (10) starts calculating the HI for t≥T. T denotes the fixed time window and F is any AE feature.

4 Results and discussion

In the following, the application of the methodologies presented in section 3 is going to be deployed in the raw SHM data acquired during the two executed test campaigns. To better demonstrate the

potential of each HI, we separate the results presentation from each campaign and show the proposed HIs for one representative SSP in sub-sections 4.1 and 4.2 for constant and variable amplitude fatigue respectively. Then, in 4.3, results for all tested coupons are shown in common Figures and for the most prominent HIs only.

4.1 Constant amplitude fatigue

4.1.1 Strain-based HIs

As mentioned in 2.3, two ways of raw data processing were implemented. The first is keeping the max absolute values at each QS loading (method 1), while the second is random sampling throughout the QS and calculating the average value (method 2). The second method is implemented in order to simulate randomness in the data acquisition e.g. in stochastic rather than deterministic loading and eliminate the effects of variable loading conditions (second test campaign). In Figure 4a, the locations of initial damage as well as the sensor positioning can be observed. The recorded strain at each sensor throughout a representative test are also presented.

Figures 4b, 4c show the extracted strains in a representative test of the first test campaign (L1-05) using pre-processing methods 1 and 2 respectively. A first observation concerns the different range of strain values. This is anticipated, since the strains extracted from the second method are the average of a uniform sampling of the whole QS, while the 1st method only uses the absolute max. On a second remark, it can be noted that the general trend of the strains remains similar in both cases. It is also worth noting that most sensors remain rather unaffected by damage i.e. the strain remains rather constant throughout the test time. The strain field around a discontinuity is only locally affected. Sensors R3 and R4 show an increase in their values which indicates that damage propagating to their vicinity is affecting their measurements.

In Figure 5, HI_1 for the two methods is presented. It can be seen that in most instances, the affected sensors display a generally increasing behavior. With the exception of R1, which shows constantly low values suggesting that the strain field near R1 remains unaffected, as compared to the reference state (t=0). The increasing values of HI_1 on all sensors is also partially attributed to the coupon's overall stiffness degradation. It is evident, however, that both methods produce similar results, demonstrating the HI's robustness regardless of the pre-processing method.

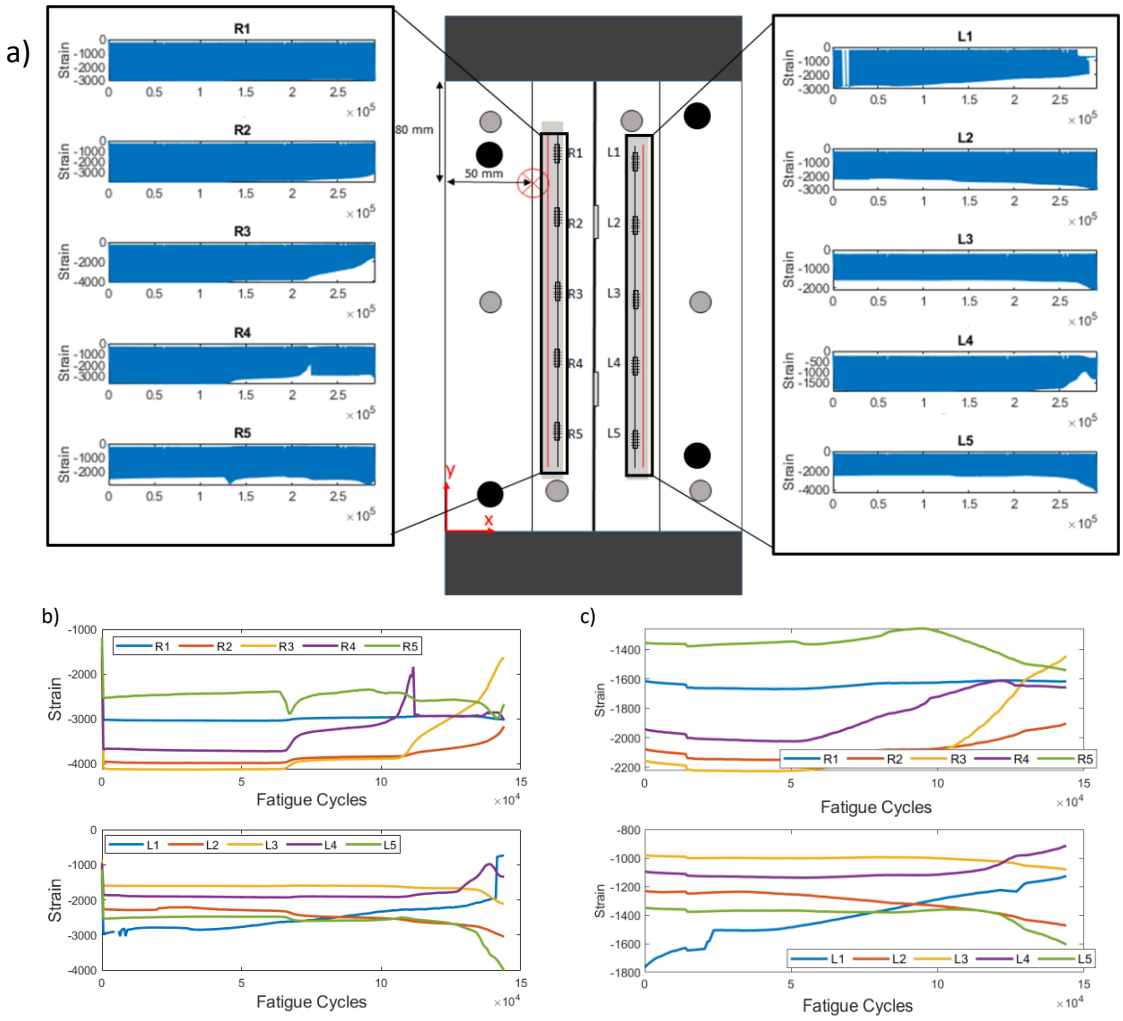

Figure 4: Constant amplitude test specimen L1-05. a) Sensor and damage locations and raw strain data for each FBG. R and L stand for right and left respectively b) max strain extracted from each quasi-static loading vs cycles (pre-processing method 1). c) random strains extracted from each quasi-static loading vs cycles (pre-processing method 2)

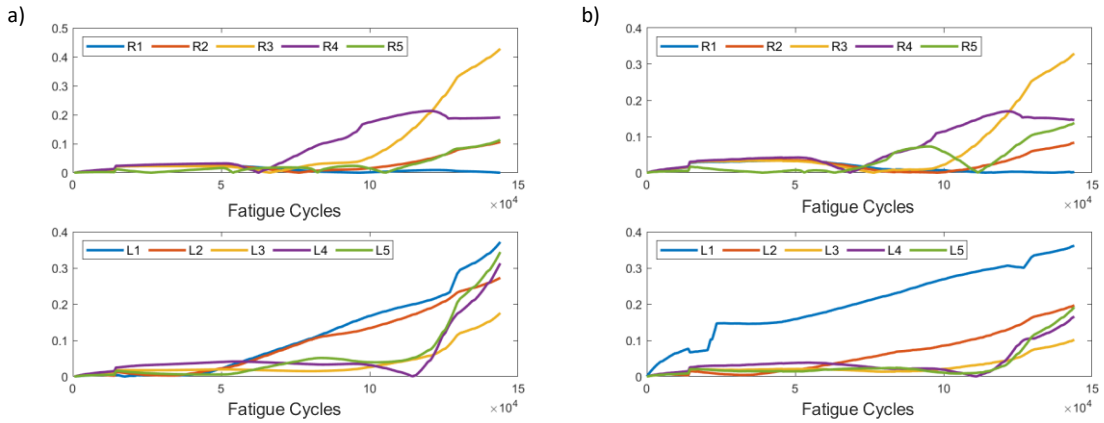

Figure 5: HI_1 progression through test cycles for the two pre-processing methods for specimen L1-05, a) method 1, b) method 2

HI_2 is shown in Figure 6. It is worth noting its behavior at the early stages. It can be seen that until almost 50k cycles, the values of most instances are low, suggesting that until that time, none of the sensors is greatly affected by damage, hence there is little effect to the respective foot's cumulative strain. After the 50k cycle mark we observe that sensors affect the cumulative strain in different ways. It is worth pointing out that sensors R3 and L1 exhibit the largest effect on the cumulative strains on their respective feet. R2, the sensor closest to the initial damage, displays the least amount of deviation, meaning that the strain field around the sensors remained almost unaffected. Also, we can comment on the consistency in the HI's behavior using the two pre-processing methods.

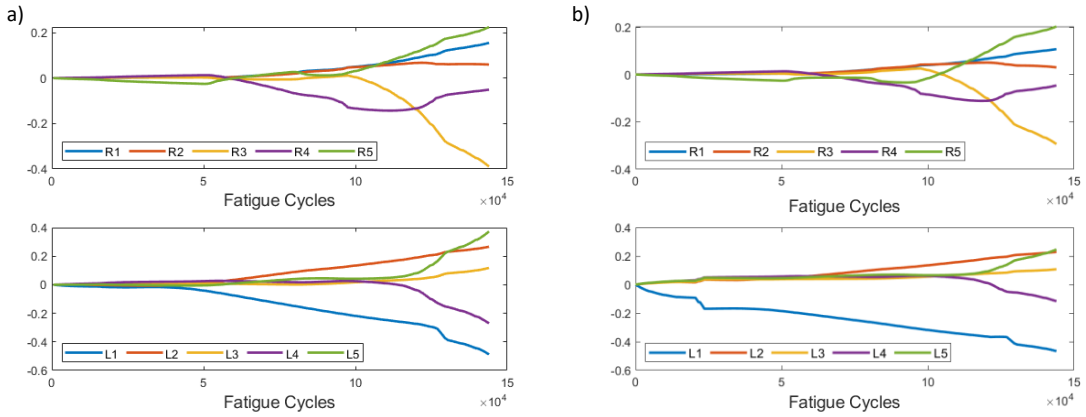

Figure 6: HI_2 progression through time for the two pre-processing methods for specimen L1-05 a) max, b) random sampling

HI_3, being a product of HI_2 displays a similar behavior. HI_3 shows, in some cases, larger deviations than HI_2 mostly due to the fact that it sums the strain readings from both feet. The larger deviations from reference state (t=0) are observed mostly after 50k cycles. The largest values are found in sensors R5 and L5 which appear to also have the largest raw strain differences. It can be observed that all instances display a clear trend. Consistency between the two pre-processing methods is also visible here.

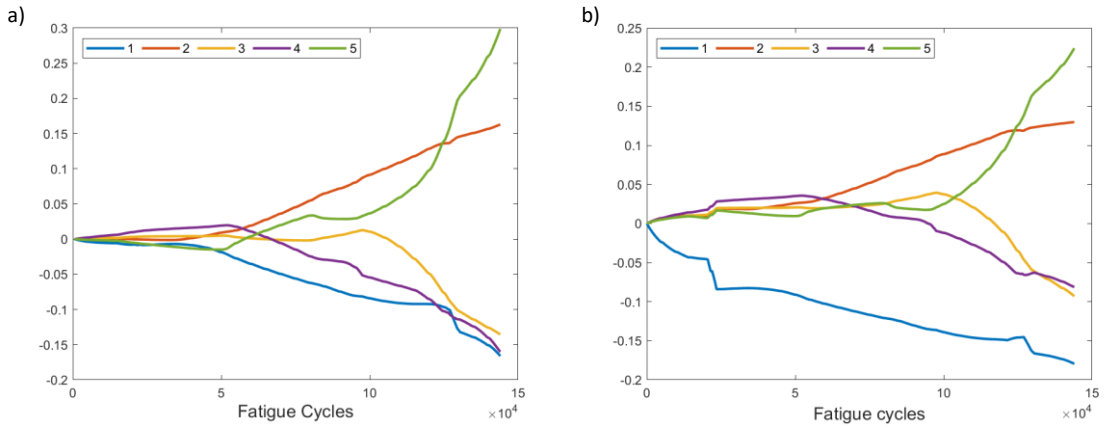

Figure 7: HI_3 progression through time for the two pre-processing methods for specimen L1-05 a) method 1, b) method 2

HI_4, as stated earlier, is an attempt to create a single HI curve fusing the ten curves of HI_1 obtained for every sensor. The behavior of HI_4 can be seen in Figure 8. A monotonically increasing trend can be observed in both versions of HI_4, highlighting its main advantage. When using processing method 1, the increasing behavior is slightly faster and more consistent, than when using method 2. However, both methods provide excellent increasing trends, demonstrating the good performance of HI_4 despite the pre-processing method employed.

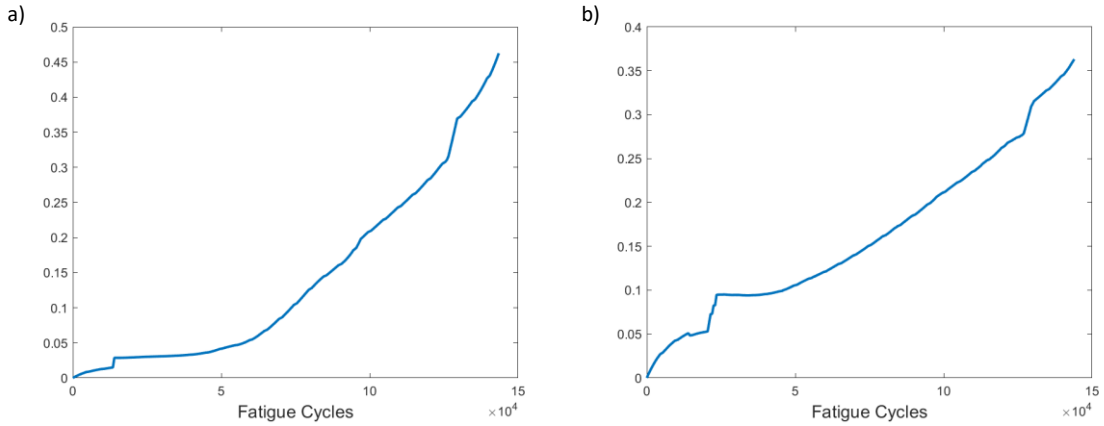

Figure 8: HI_4 progression through time for the two pre-processing methods for specimen L1-05 a) method 1, b) method 2

The first of the virtual health indicators, vHI_1 is presented in Figure 9. At first the HI was calculated separately for each foot to observe the differences in behavior. What was observed and can be more clearly seen in Figure 9-b is that the HI is affected by "aggressive" behaviors, like the one from sensor L1. As evidenced in Figure 5b, sensor L1 shows an "aggressive" increase in values unlike any other sensor. This is also projected in vHI_1, where the left foot instance of method 2 decreases faster than in method 1. Hence, we investigated what the effect is if the indicator is calculated jointly for both feet, i.e. instead of calculating vHI_1 for left and right foot FBGs separately, it was calculated for all ten FBG sensors combined. The result displays a more gradual behavior than that of the left foot, while also retaining aspects of both feet. This was also the case for the rest of the specimens. To focus on the results of Figure 9 we observe that the indicator decreases gradually from 1 to 0.2, when the specimen fails. The consistency between the two pre-processing methods

is slightly diminished, however, due to the nature of vHI_1, a desirable monotonic behavior is achieved with both methods.

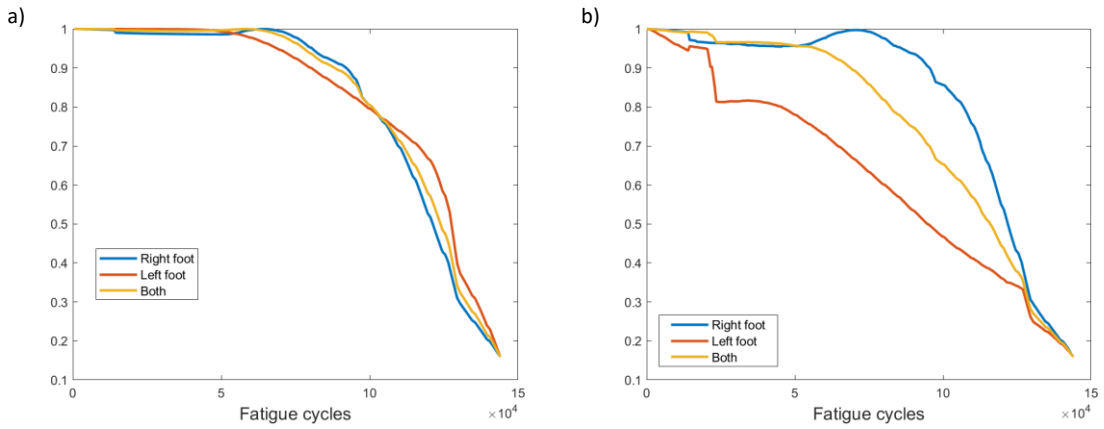

Figure 9: vHI_1 progression through time for the two pre-processing methods for specimen L1-05 a) method 1, b) method 2

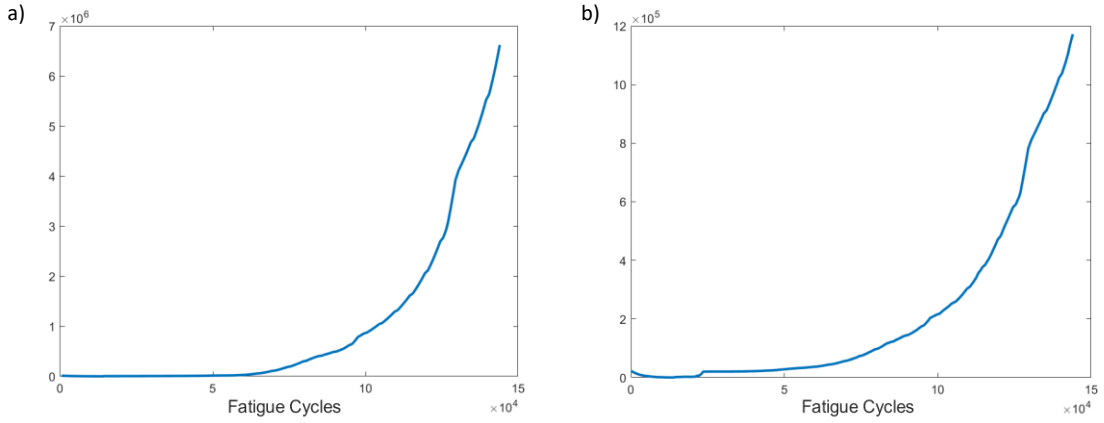

Figure 10: vHI_2 progression through time for the two pre-processing methods for specimen L1-05 a) method 1, b) method 2

VHI_2 is PCA's sum of reconstructed residual squared error, i.e. Q index, and is depicted in Figure 10. At a first glance we note the difference in the range of vHI_2 values between the two pre-processing methods. Method 1 has much larger values that method 2. This is to be expected, and was previously observed, due to the higher original strain values use for the PCA model. Other than the scale differences, the two curves display similar trends of very high monotonicity, gradually increasing in time, a promising result for use in failure prognostic tasks.

4.1.2 AE based HIs

As we mentioned previously, AE was constantly being recorded throughout the total duration of the tests. In Figure 11, the amplitude vs cycles can be observed. Initially, AE is high since the initial damage starts very soon to propagate (Stage I). After the first evolution, the initial damage is better accommodated by the structure through stress redistribution and does not grow significantly reducing the acoustic activity until later stages of the experiment (Stage II). In the final stage (Stage

III), the damage is starting to grow once more leading to the final failure, which is indicated by the extensive acoustic activity.

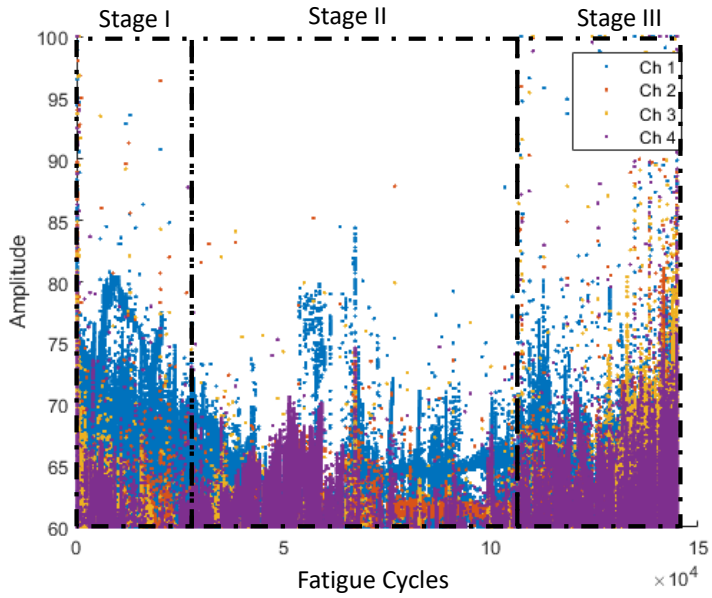

Figure 11: Amplitude vs cycles for all the different AE channels for specimen L1-05 (stages are qualitatively drawn)

Two HIs are extracted from the acoustic emission data, the windowed cumulative hits and RA. The resulted curves display an increasing trend especially near the end of life. In the early stage, both features display slightly higher values due to the early damage growth, and in the middle stage a drop in values is observed and thereafter the values remain almost constant. Near the end of life (EoL), the HIs display a sudden increase which is also visible in the amplitude graph. It is evident that this specimen does not have high monotonicity, but it will be shown later that other specimens display more promising behaviors. However, worth mentioning again is that near the EoL an increasing trend is observed.

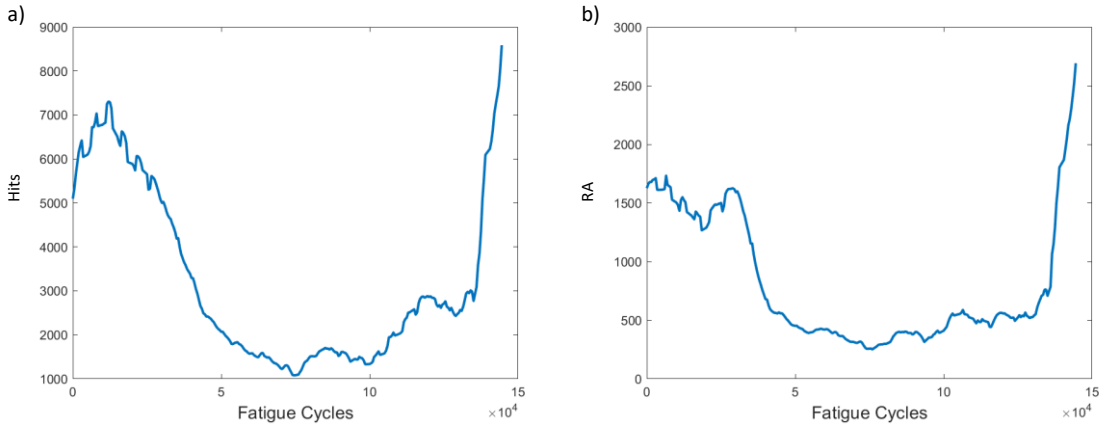

Figure 12: (a) windowed cumulative hits and (b) RA for window size of 500 cycles for specimen L1-05

4.2 Variable amplitude fatigue

4.2.1 Strain-based HIs

Similar to the constant amplitude test campaign, the same data processing techniques were applied and are presented. A representative specimen (L1-06) is shown in Figure 13a with the sensor positioning and the initial damage (impact) location. The data recorded at each sensor are also presented. The load increases are evident by the increase in the strain values. Also, it is important to note that sensor L1 is disbonded from the early stages of the test, while L5 and R5 disbond near the final stage. This can be deducted, apart from visual inspection, from the significant change in the strains. These data were considered in the following steps, to display the robustness of our HIs. The extracted strains, using the two processing methods can be seen in Figure 13 b and c.

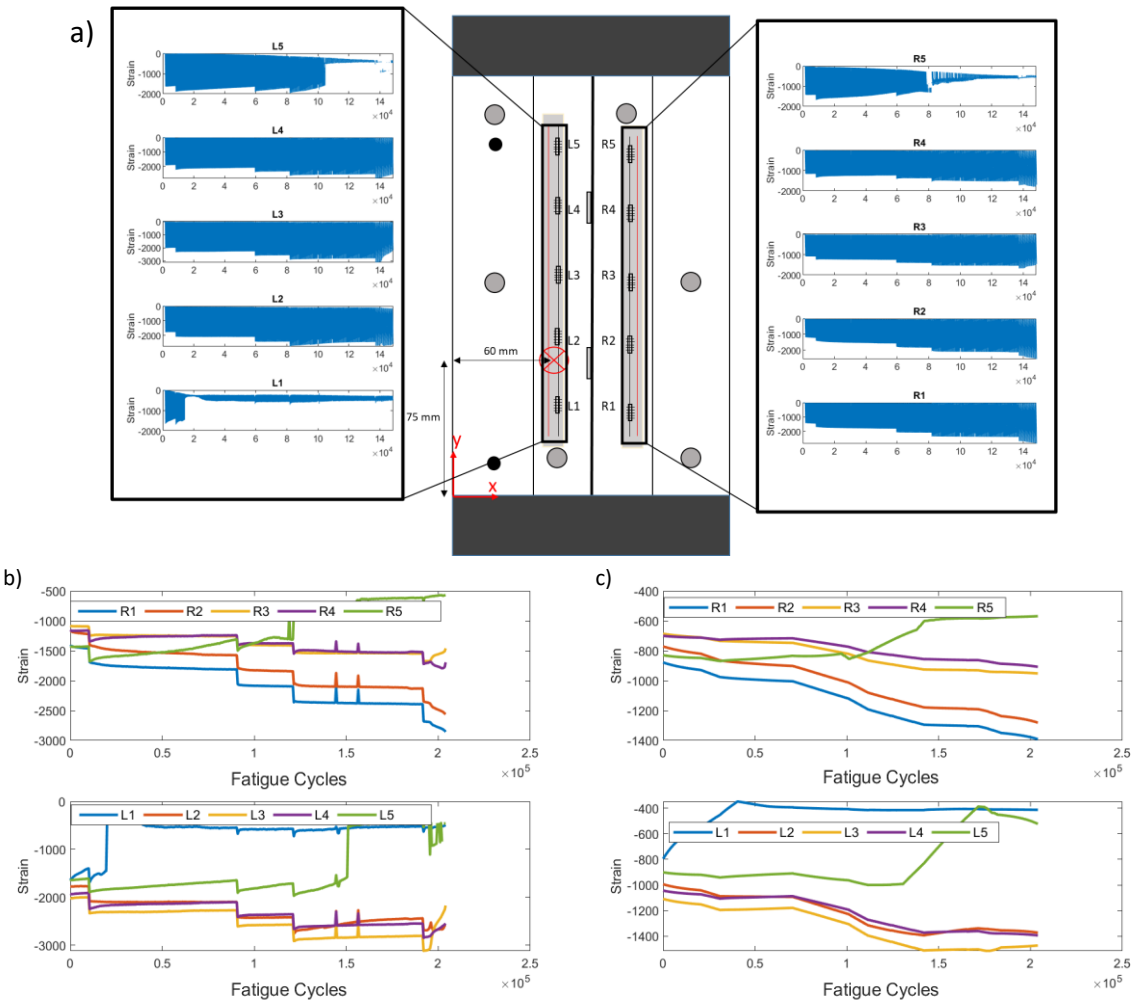

Figure 13: Variable amplitude test specimen L1-06. a) Sensor and damage locations and raw strain data for each FBG. b) extracted max data from each Quasi-static vs cycles (pre-processing method 1). c) extracted mean data for each Quasi-static vs cycles (pre-processing method 2)

In method 1, the load changes can be clearly seen at the discontinuities (jumps) in strain values. This behavior shall definitely affect the HIs performance giving instantaneous changes that might be erroneously attributed to damage. On the other hand, method 2 alleviates this behavior proving

that the main objective for introducing this method is achieved. To provide a clearer comparison with the constant amplitude test analyses, the curves from method 1 are also smoothened before extracting the HIs. This will eliminate the load effect, but as it has been observed in the constant amplitude fatigue, the HIs appear to be robust, showing similar results regardless of the input data.

HI_1 for both methods is presented in Figure 14. As was previously stated the two methods have slight differences is scale, with method 1 exhibiting larger values. The general behavior of the HI remains the same in both data processing methods, and HI_1 displays an increasing behavior over time.

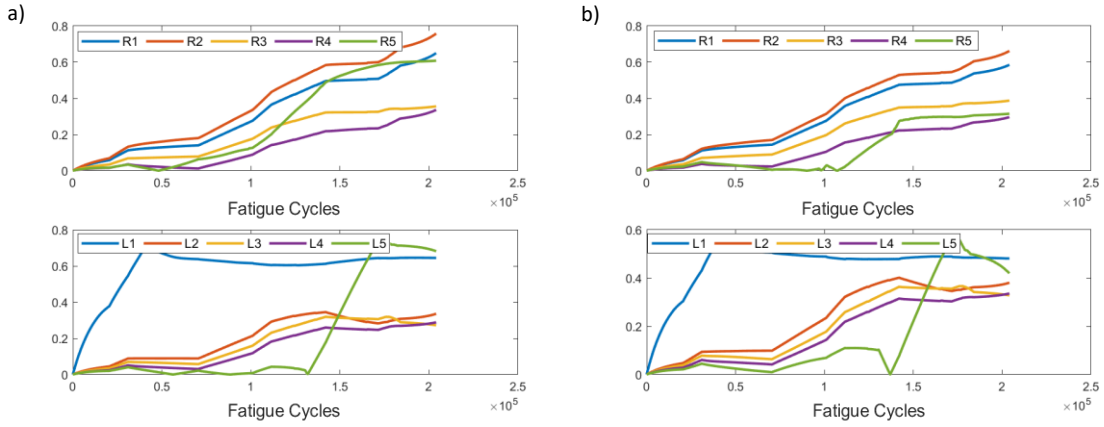

Figure 14: HI_1 progression through time for the two pre-processing methods for specimen L1-06 a) method 1, b) method 2

HI_2 displays similar trends with those seen in the constant amplitude fatigue campaign. The HI is slowly increasing until the 40k cycle mark where the curves for sensors R1, R2 and R5 start to rapidly diverge, while R3 and R4 remain rather constant throughout the entire lifetime. The left foot sensors increase until 40k cycles and then remain constant up until 130k where L1-L3 increase and L5 starts decreasing. In method 2, the right foot sensors display significantly lower values than their method 1 counterparts, but the overall behaviors are similar. R5 and L5 even before disbonding contribute the most to the cumulative strains.

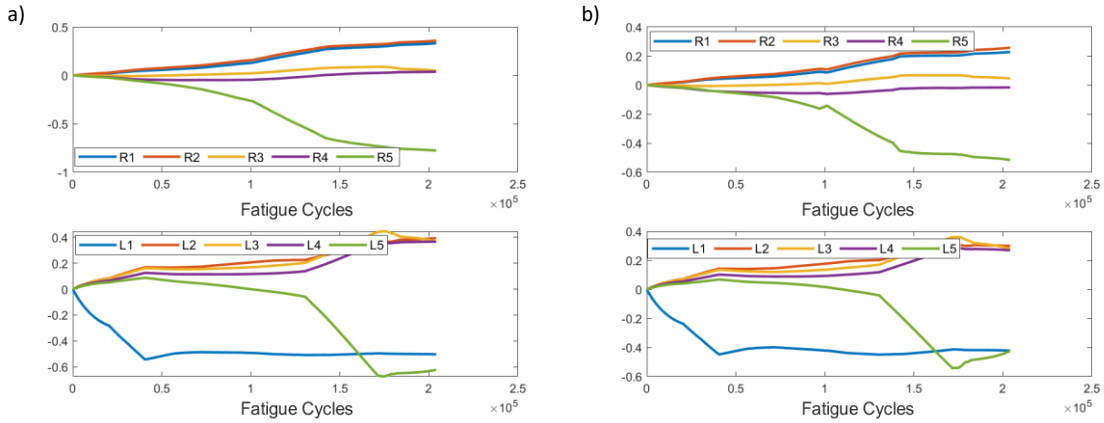

Figure 15: HI_2 progression through time for the two pre-processing methods for specimen L1-06 a) method 1, b) method 2

HI_3 shows a similar trend as HI_2. Unlike HI_2, the different sensors diverge from the very start. Also, worth noting is that up to the point of disbonding, R5 and L5 show the larger increase in values, and after the disbond they remain almost constant. All sensors display similar trends in both methods.

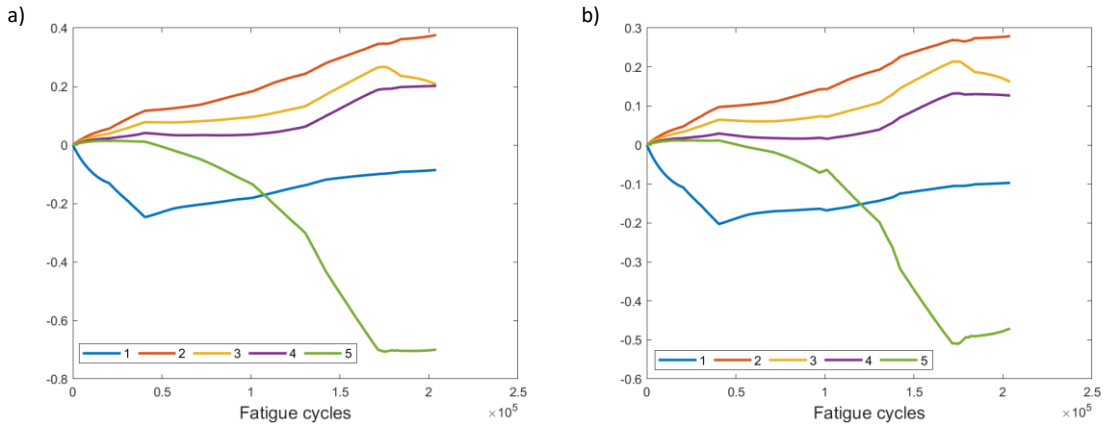

Figure 16: HI_3 progression through time for the two pre-processing methods for specimen L1-06 a) method 1, b) method 2

HI_4 shows almost identical behavior in both methods. A monotonous trend increasing over time with a few constant slopes in the beginning and near the end is shown. HI_4 shows larger values when using method 1 for preprocessing, an expected outcome, since the max values of the strain are higher. Once again, the main attribute of the HI, i.e. monotonicity, is achieved.

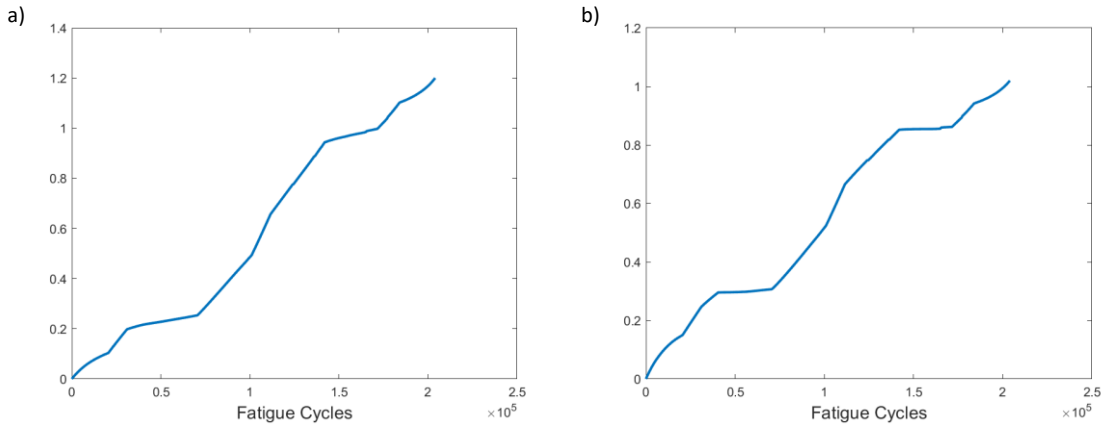

Figure 17: HI_4 progression through time for the two pre-processing methods for specimen L1-06 a) method 1, b) method 2

VHI_1 displays a gradually decreasing behavior from 1 to 0.2 (Figure 18). Again, using all sensors to calculate the HI provides a similar behavior to the average of the two feet independently and in this particular specimen, eliminates the increase observed at the final moments in the left foot case. A good trend overall is displayed when using this HI in variable amplitude fatigue, regardless of the data processing method.

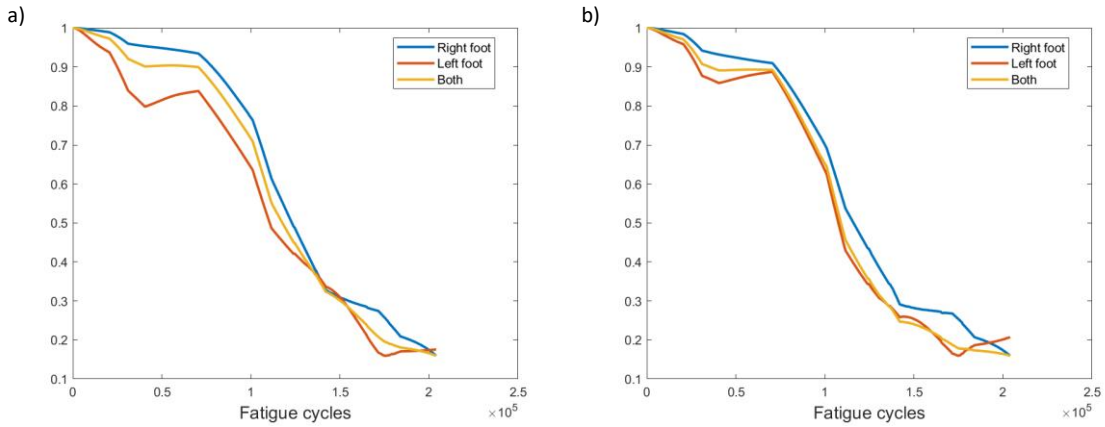

Figure 18: vHI_1 progression through time for the two pre-processing methods for specimen L1-06 a) method 1, b) method 2

Q index (vHI_2) shows an increasing trend over time. The major difference between the two pre-processing methods is the scale of the HI. Other than that, no major differences are noted. A gradually increasing trend, which increases faster after 60k cycles is observed. It should be noted that this indicator provides a promising trend for prognostics, regardless of processing method and experimental conditions.

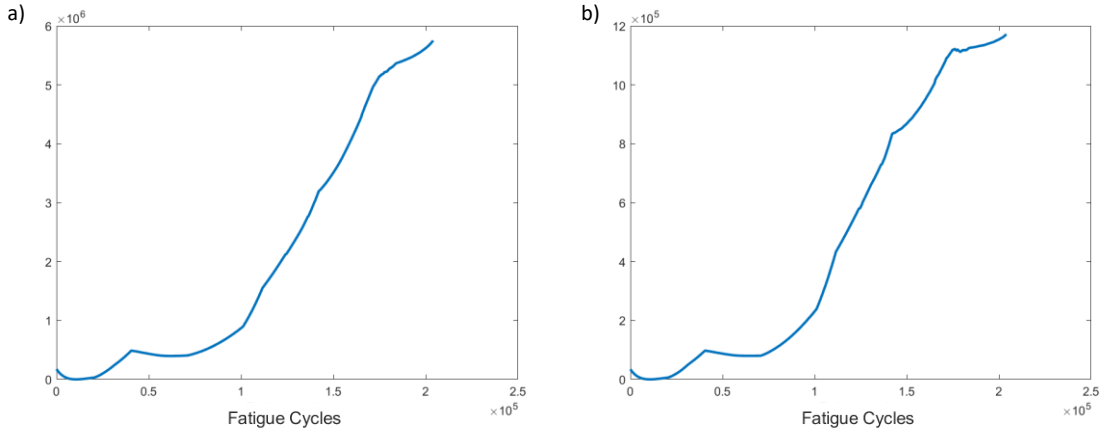

Figure 19: vHI_2 progression through time for the two pre-processing methods for specimen L1-06 a) method 1, b) method 2

The first step to evaluate the suitability of the various HIs is to see how well they correlate with damage growth. To this direction, we utilize the evidence acquired by the phased array C-scans that were performed at several occasions throughout each test. The three single curve HIs accompanied by the phased array images are used. The images depict the damage area, i.e. the location of the impact on the stringer's foot. Also, to further demonstrate the capabilities of the HIs as well as the data pre-processing methods, method 2, i.e. random sampling method, is used for this visualization. The damage size was also approximated using ImageJ [39]. ImageJ can measure pixel density and correlate pixel count with a known distance. From Figure 20 it is evident that there is correlation between the damage growth and HIs. The first phased array image is right after the impact was performed, i.e. at 0 cycles. After 10k cycles it can be observed that the damage has only slightly grown and has been captured both by HI 1f and HI 4. Q index (vHI_2) at 10k cycles still displays values close to 0. The large increase in the HI values after the 10k mark is attributed to the

increase to the load. At 90k cycles, it is evident that the damage has grown (tail at the bottom side is larger) and this is also depicted in the HIs' behaviors. At this point (90k cycles) the HIs start to rapidly increase in contrast to previous time points, where the increase was much slower, and so was the damage growth. From 90-120k the tail of the impact damage continues to grow and a rapid change in the HIs' values is accompanying this growth. In the final image, the damage growth is significant, yet it is still contained in the bottom area. The damage has grown both horizontally and vertically, which has not been the case previously (the growth was mostly vertical). The HIs increase has declined in rate, meaning that when reaching that point the damage has already grown and the growth is lower during the final cycles before catastrophic failure.

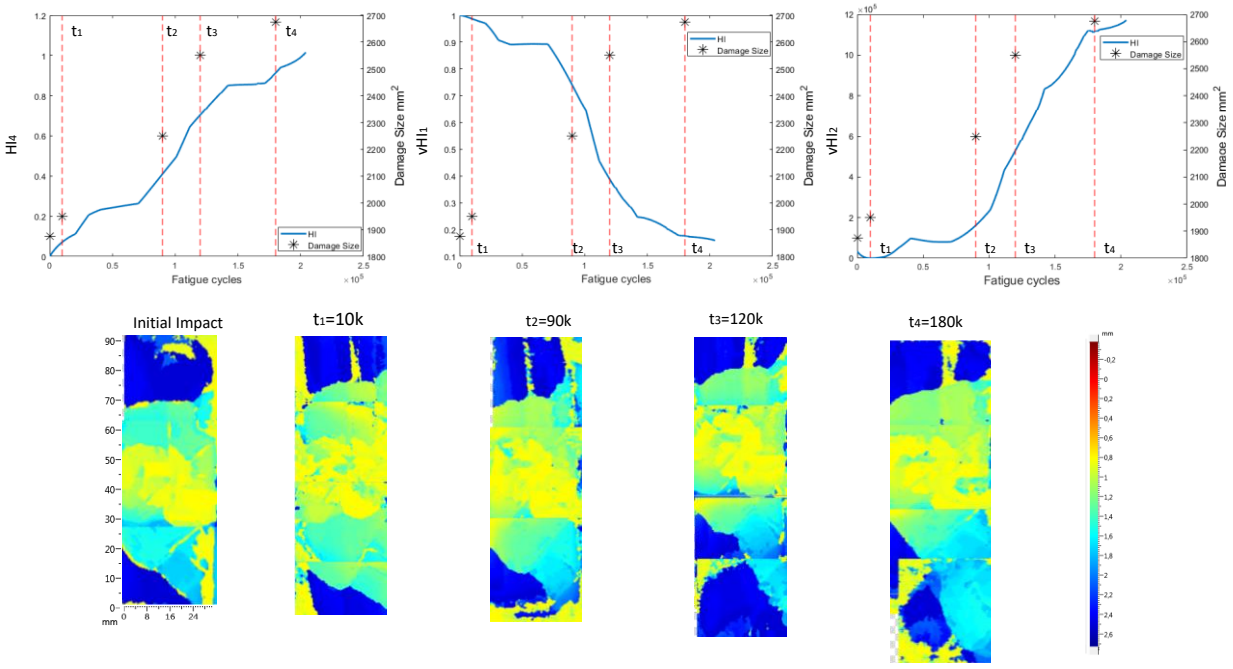

Figure 20: Phased array C-scan images at various instances of the L1-06 experiment alongside HI_4, vHI_1 and vHI_2 progression through time. The red dashed lines indicate the time of measurement.

4.2.2 AE based HIs

The AE amplitude versus the fatigue cycles can be seen in Figure 21. Acoustic activity presents a constant band between 62 and 72 dB throughout the entirety of the experiment suggesting that the preexisting damage produces significant acoustic emission. Also, worth noting is the slightly higher amplitudes in the early stages. Similar to the constant amplitude fatigue, even at lower loads the preexisting damage appears to cause some shifts between the broken layers in the composite, yet not enough for the damage to grow (Stage I). Near the EoL (Stage III), the AE amplitude is significantly increased especially during the final moments of the experiment, where a constant amplitude band from 62-100 dB is seen.

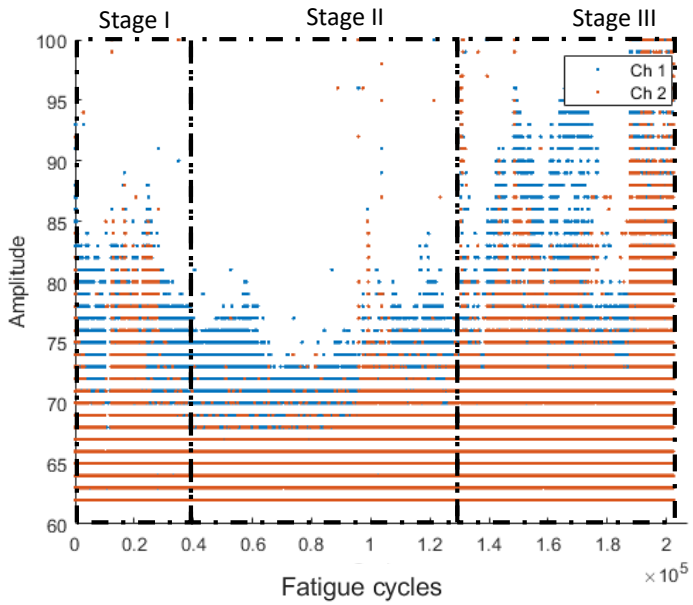

Figure 21: Amplitude vs fatigue cycles for specimen L1-06 (stages are qualitatively drawn)

The windowed cumulative features used as HIs, display an increasing trend over the course of the specimen's lifetime. A slowly decreasing behavior can be seen in the early stages, and a rapid increase is observed during the later stages of the fatigue experiments. Both features, display promising attributes and constitute potential candidates for diagnostic and prognostic purposes.

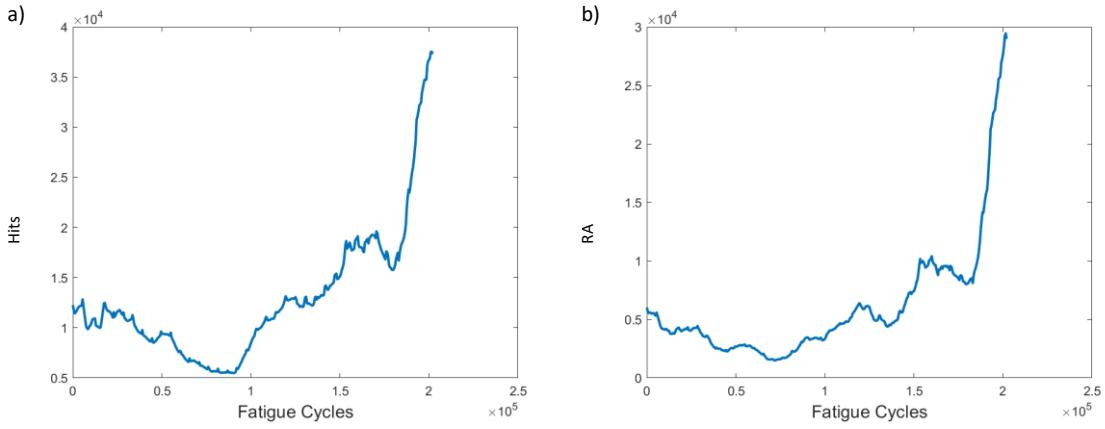

Figure 22: (a) windowed cumulative hits and (b) RA vs fatigue cycles for specimen L1-06

4.3 Discussion

Several health indicators for both constant and variable amplitude fatigue have been proposed and their performance was presented throughout fatigue tests. The strain based HIs, i.e. HI_1, HI_2, and HI_3 have been used in [7] to detect damage successfully in quasi-static numerical tests. In the present study, these indicators do not provide such information, since through time they constantly increase. However, this is not the scope of this research. The HIs investigated in the present work here are intended for diagnostic and prognostics tasks where monotonic trends are highly desirable.

In Figure 23a-c three HIs, i.e. HI_4, vHI_1 and vHI_2, are presented comparatively for the specimens of both experimental campaigns. Since, as we previously noted, both data processing methods provide similar results, method 2 is used to depict these comparisons. The random sampling method is favorable to deal with effects of different loads and display the robustness of these HIs in different loading conditions. HI_4 is shown in Figure 23a. Monotonicity is achieved in all specimens throughout the lifetime. Though monotonicity and similar behaviors are highly desirable attributes, a concern is presented in the form of lack of common failure values (i.e. poor prognosability). Similar attributes are observed in the behavior of Q index, high monotonicity, but poor prognosability. Higher variability is observed in Q index though, due to the much higher overall values. vHI_1 displays a decreasing trend whose range is restricted by the radial basis function normalization. It should be noted however, that vHI_1 requires a priori knowledge of the minimum and maximum values, for the normalization. It is presented as a concept and due to the extremely promising decreasing trend it possesses. As previously stated, a solution to this drawback is the inference of min and max values from a training dataset.

The HIs, combined with the data pre-processing techniques, provide overall good monotonicity for all specimens in the current study, highlighting their ability to do so despite the different loading scenarios in the two test campaigns. This also shows the robustness of the proposed HIs. As far as HI_2 and HI_3 are concerned, in their current form they lack trendability as every sensor give its own indicator. Opposing trends are evidenced, depending on the sensor studied and even looking at the same sensor on two different specimens it is not guaranteed that the behavior will be similar, since the buckling modes may affect the local behavior as well. However, these HIs provide useful information regarding the damage progression, as seen in [7] by successfully monitoring disbond growth. It is worth pointing out that HI_2 and HI_3 curves start to diverge when damage is becoming significant. This can prove useful as an alarm of when to launch the prognostic task.

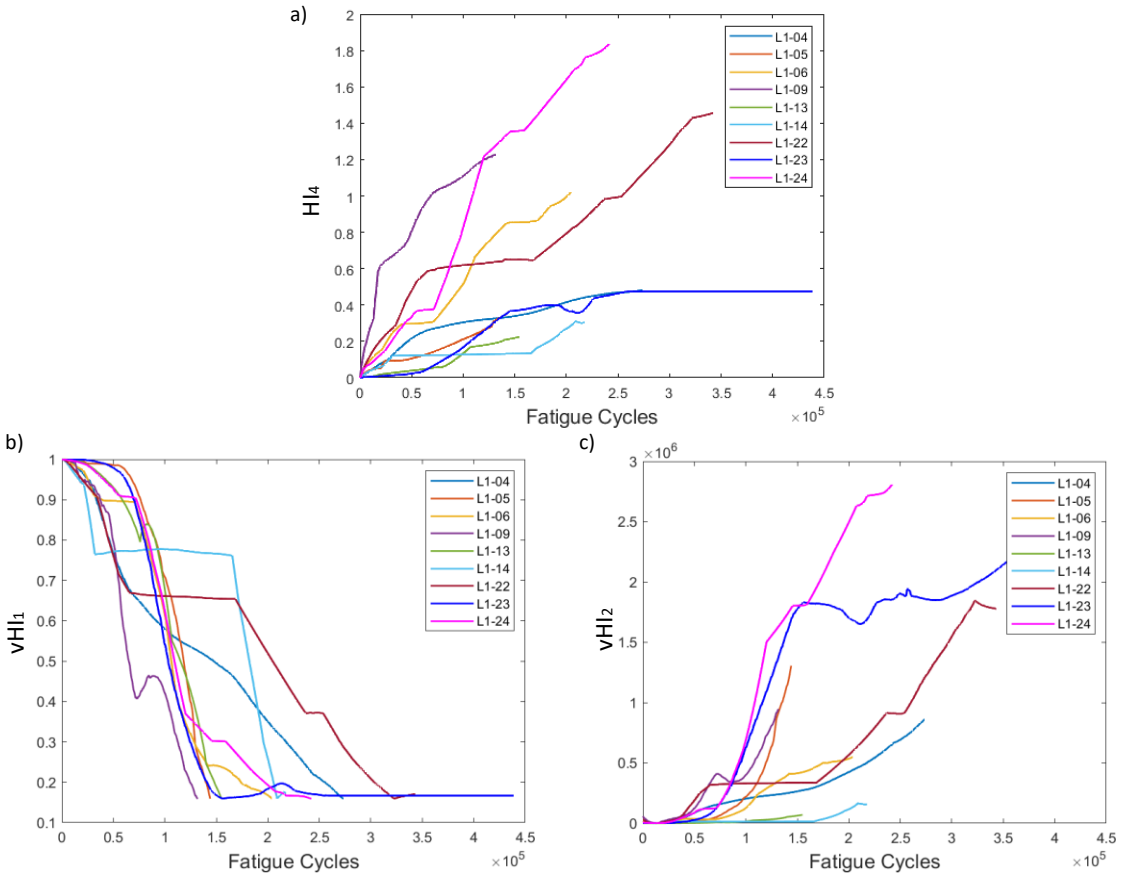

Figure 23 : a) HI_4, b) vHI_1, c) vHI_2 comparisons for all tested specimens

AE-based HIs are presented in Figure 24 for all specimens of the study. Most specimens display increasing behaviors over time for both cumulative hits and RA. Interestingly and unlike the strain based HIs, the failure values of the AE-based HIs have high prognosability, making it easier to set a failure threshold. Not all specimens, however, are able to reach this threshold, but in prognostics a variety of degradation histories is necessary for greater accuracy and account of more degradation scenarios.

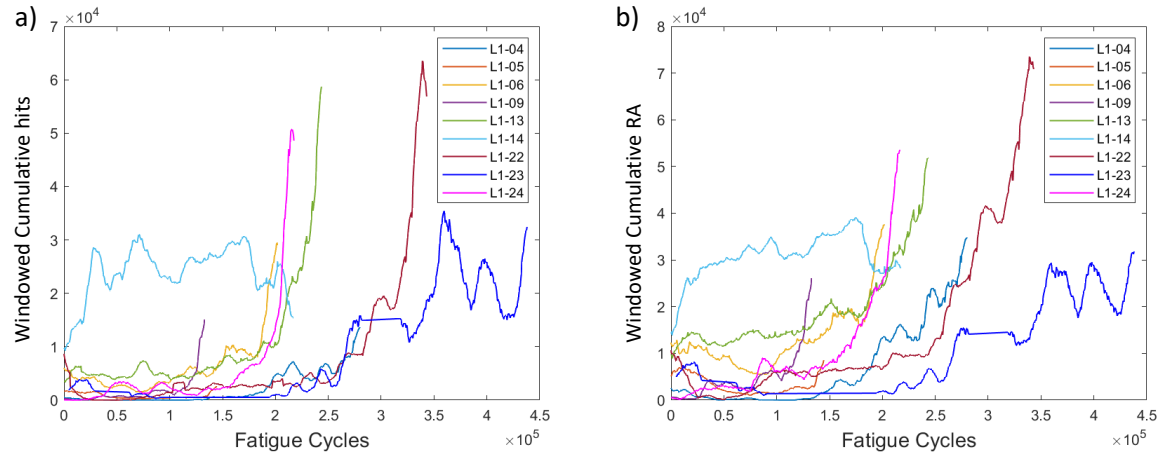

Figure 24: (a) windowed cumulative hits and (b) windowed cumulative RA for all specimens

5 Conclusion

In the present work, several new Health Indicators are proposed and extracted from raw acoustic emission and strain data recorded after two fatigue test campaigns of stiffened composite panels. Constant as well as variable amplitude compression-compression fatigue tests were conducted with quasi-static loadings performed periodically. Two strain data pre-processing strategies were examined, to evaluate and show the performance of the various health indicators under different loading conditions. The random sampling across the quasi-static loading proved equally efficient in producing highly monotonic HIs while eliminating variable loading effects (discontinuities in the HI behavior).

Three physical and two virtual HIs based on PCA are proposed to extract from the raw strain data. The proposed HIs display monotonic trends, mostly increasing throughout the specimens' lifetime, managing to correlate with the degradation process as verified by the phased-array C-scans. It was also shown that the HIs have increased trendability i.e. they show similar behaviors for both groups of tested specimens, despite the different loading conditions. Also, HI_4, vHI_1 and vHI_2 displayed high monotonic behaviors, highly desirable for prognostics, while the HI_2 and HI_3 can provide an alarm threshold for prognostics initiation. The main drawback of the strain-based HIs is the rather poor prognosability, which make it challenging to set a universal failure threshold.

Two AE-based HIs were extracted, i.e. windowed cumulative hits and windowed cumulative RA. Both HIs possess monotonicity lower though than the strain-based HIs but displayed higher prognosability. AE-based HIs are independent of the loading conditions From the discussion above and the pros and cons of both groups of HIs, it becomes apparent that the proposal of fused HIs (feature-level data fusion) has the potential to enhance the pros and alleviate the cons. This is in our imminent plans for future work as well as the implementation for the proposed HIs for prognostication of the remaining useful life.

Acknowledgements

The authors would like to acknowledge Embraer for the design of the SSCs, Optimal Structural Solutions for the manufacturing of the SSCs, Smartec for the SMARTapes procurement, and our colleagues at the University of Patras and Delft University of Technology for their technical support.

Funding

This work was financially supported by the European Union's Horizon 2020 research and innovation programme ReMAP (Grant Agreement Number: 769288).

References

1. Kassapoglou C. *Design and analysis of composite structures: with applications to aerospace structures*. John Wiley & Sons, 2013.
2. Andreades C, Meo M and Ciampa F. Fatigue testing and damage evaluation using smart CFRP composites with embedded PZT transducers. *Materials Today: Proceedings*. 2021; 34: 260-5.
3. Marques R, Unel M, Yildiz M and Suleman A. Remaining useful life prediction of laminated composite materials using thermoelastic stress analysis. *Composite Structures*. 2019; 210: 381-90.

4. Loutas T, Eleftheroglou N and Zarouchas D. A data-driven probabilistic framework towards the in-situ prognostics of fatigue life of composites based on acoustic emission data. *Composite Structures*. 2017; 161: 522-9.
5. Eleftheroglou N and Loutas T. Fatigue damage diagnostics and prognostics of composites utilizing structural health monitoring data and stochastic processes. *Structural Health Monitoring: An International Journal*. 2016; 15: 473-88.
6. Grassia L, Iannone M, Califano A and D'Amore A. Strain based method for monitoring the health state of composite structures. *Composites Part B: Engineering*. 2019; 176: 107253.
7. Milanoski DP and Loutas TH. Strain-based health indicators for the structural health monitoring of stiffened composite panels. *Journal of Intelligent Material Systems and Structures*. 2020: 1045389X20924822.
8. Palaniappan J, Ogin SL, Thorne AM, et al. Disbond growth detection in composite–composite single-lap joints using chirped FBG sensors. *Composites Science and Technology*. 2008; 68: 2410-7.
9. Li HCH, Beck F, Dupouy O, et al. Strain-based health assessment of bonded composite repairs. *Composite Structures*. 2006; 76: 234-42.
10. Kahandawa GC, Epaarachchi J, Wang H and Lau KT. Use of FBG Sensors for SHM in Aerospace Structures. *Photonic Sensors*. 2012; 2: 203-14.
11. Sundaram R, Kamath G, Gupta N and Rao MS. Structural health monitoring of co-cured composite structures using FBG sensors. *Smart Structures and Materials 2005: Smart Structures and Integrated Systems*. International Society for Optics and Photonics, 2005, p. 559-70.
12. Takeda S-i, Aoki Y and Nagao Y. Damage monitoring of CFRP stiffened panels under compressive load using FBG sensors. *Composite Structures*. 2012; 94: 813-9.
13. Airoldi A, Bettini P, Belotti P, Loutas T, Koimtzoglou C and Sala G. Design of health and usage monitoring systems based on optical fibers for composite wing spars. *Proceedings of 28th ICAF Symposium, Helsinky*. 2015, p. 3-5.
14. Sbarufatti C, Corbetta M, San Millan J, Frovel M, Stefaniuk M and Giglio M. Model-assisted performance qualification of a distributed SHM system for fatigue crack detection on a helicopter tail boom. *EWSHM, Bilbao*. 2016.
15. Sbarufatti C, Manes A and Giglio M. Performance optimization of a diagnostic system based upon a simulated strain field for fatigue damage characterization. *Mechanical Systems and Signal Processing*. 2013; 40: 667-90.
16. Tur M, Bosboom MB, Evenblij R, et al. Fiber-optic based HUMS concept for large aircraft structure based on both point and distributed strain sensing. *8th European Workshop on Structural Health Monitoring*. 2016.
17. Guemes A, Sierra-Pérez J, Rodellar J and Mujica L. A robust procedure for Damage detection from strain measurements based on Principal Component Analysis. *Key Engineering Materials*. Trans Tech Publ, 2013, p. 128-38.
18. Guemes A, Fernandez-Lopez A, P FD-M, Lozano A and Sierra-Perez J. Structural Health Monitoring in Composite Structures by Fiber-Optic Sensors. *Sensors*. 2018; 18.
19. Saeedifar M and Zarouchas D. Damage characterization of laminated composites using acoustic emission: A review. *Composites Part B: Engineering*. 2020: 108039.
20. Zhou W, Lv Z-h, Li Z-y and Song X. Acoustic emission response and micro-deformation behavior for compressive buckling failure of multi-delaminated composites. *The Journal of Strain Analysis for Engineering Design*. 2016; 51: 397-407.
21. Masmoudi S, El Mahi A and Turki S. Fatigue behaviour and structural health monitoring by acoustic emission of E-glass/epoxy laminates with piezoelectric implant. *Applied Acoustics*. 2016; 108: 50-8.

22. Carmi R, Wisner B, Vanniamparambil PA, Cuadra J, Bussiba A and Kontsos A. Progressive Failure Monitoring of Fiber-Reinforced Metal Laminate Composites Using a Nondestructive Approach. *Journal of Nondestructive Evaluation, Diagnostics and Prognostics of Engineering Systems*. 2019; 2.
23. Liu Y, Mohanty S and Chattopadhyay A. A Gaussian process based prognostics framework for composite structures. *Modeling, Signal Processing, and Control for Smart Structures 2009*. International Society for Optics and Photonics, 2009, p. 72860J.
24. Broer A, Galanopoulos G, Benedictus R, Loutas T and Zarouchas D. Fusion-based damage diagnostics for stiffened composite panels. (in press). *Structural Health Monitoring*. 2021.
25. Loutas T, Eleftheroglou N, Georgoulas G, Loukopoulos P, Mba D and Bennett I. Valve Failure Prognostics in Reciprocating Compressors Utilizing Temperature Measurements, PCA-Based Data Fusion, and Probabilistic Algorithms. *IEEE Transactions on Industrial Electronics*. 2020; 67: 5022-9.
26. Eleftheroglou N, Zarouchas D, Loutas T, Alderliesten R and Benedictus R. Structural health monitoring data fusion for in-situ life prognosis of composite structures. *Reliability Engineering & System Safety*. 2018; 178: 40-54.
27. Hu C, Youn BD, Wang P and Yoon JT. An ensemble approach for robust data-driven prognostics. *International Design Engineering Technical Conferences and Computers and Information in Engineering Conference*. American Society of Mechanical Engineers, 2012, p. 333-47.
28. Wen P, Zhao S, Chen S and Li Y. A generalized remaining useful life prediction method for complex systems based on composite health indicator. *Reliability Engineering & System Safety*. 2021; 205: 107241.
29. Eleftheroglou N, Zarouchas D, Loutas T, Alderliesten RC and Benedictus R. Online remaining fatigue life prognosis for composite materials based on strain data and stochastic modeling. *Key Engineering Materials*. Trans Tech Publ, 2016, p. 34-7.
30. Milanoski D, Galanopoulos G, Broer A, Zarouchas D and Loutas T. A Strain-Based Health Indicator for the SHM of Skin-to-Stringer Disbond Growth of Composite Stiffened Panels in Fatigue. *European Workshop on Structural Health Monitoring*. Springer, 2020, p. 626-35.
31. Loukopoulos P, Zolkiewski G, Bennett I, et al. Reciprocating compressor prognostics of an instantaneous failure mode utilising temperature only measurements. *Applied Acoustics*. 2019; 147: 77-86.
32. Zhang Z, Wang Y and Wang K. Intelligent fault diagnosis and prognosis approach for rotating machinery integrating wavelet transform, principal component analysis, and artificial neural networks. *The International Journal of Advanced Manufacturing Technology*. 2013; 68: 763-73.
33. Shahid N and Ghosh A. TrajecNets: Online Failure Evolution Analysis in 2D Space. *United Technologies Research Center, Penrose Wharf, Penrose Business Center, Cork, Ireland*. 2019.
34. Inaudi D and Glisic B. Development of distributed strain and temperature sensing cables. *17th International Conference on Optical Fibre Sensors*. International Society for Optics and Photonics, 2005, p. 222-5.
35. Sierra-Pérez J, Güemes A, Mujica LE and Ruiz M. Damage detection in composite materials structures under variable loads conditions by using fiber Bragg gratings and principal component analysis, involving new unfolding and scaling methods. *Journal of Intelligent Material Systems and Structures*. 2015; 26: 1346-59.
36. Ahmed M, Gu F and Ball A. Fault detection of reciprocating compressors using a model from principles component analysis of vibrations. *Journal of Physics: Conference Series*. IOP Publishing, 2012, p. 012133.

37. Milanoski DP and Loutas TH. Strain-based damage assessment of stiffened composite panels for structural health monitoring purposes. *9th thematic conference on smart structures and materials, Paris*. 2019, p. 8-11.
38. Javed K, Gouriveau R, Zerhouni N and Nectoux P. Enabling health monitoring approach based on vibration data for accurate prognostics. *IEEE Transactions on industrial electronics*. 2014; 62: 647-56.
39. Abràmoff MD, Magalhães PJ and Ram SJ. Image processing with ImageJ. *Biophotonics international*. 2004; 11: 36-42.